Catalysis Science & Technology

Accepted Manuscript

Catalysis
Science &
Technology

www.rsc.org/catalysis

Volume 6 | Number 1 | 7 January 2016 | Pages 1–308

ISSN 2044-4753

ROYAL SOCIETY OF CHEMISTRY

PAPER
Qingzhu Zhang et al.
Catalytic mechanism of C–F bond cleavage: insights from QM/MM analysis of fluoroacetate dehalogenase

175 YEARS

ROYAL SOCIETY OF CHEMISTRY

rsc.li/catalysis

Journal Name

ARTICLE

Designing a novel dual bed reactor to realize efficient ethanol synthesis from dimethyl ether and syngas

Xinhua Gao,[a,b] Bolian Xu,[c] Guohui Yang,[b] Xiaobo Feng,[b] Yoshiharu Yoneyama,[b] Ushio Taka[d] and Noritatsu Tsubaki*[b]

A novel dual bed reactor packed with the combination of zeolite (H-Modernite or H-Ferrierite) catalyst and CuZnAl catalyst was proposed to realize the direct ethanol (EtOH) synthesis from dimethyl ether (DME) and syngas (CO + H$_2$). DME and CO were firstly introduced into the upper zeolite bed to conduct the carbonylation reaction, and then H$_2$ was directly imported into the below CuZnAl catalyst bed to accomplish the hydrogenation of methyl acetate (MA) produced at the first catalyst bed. In this novel dual bed process, the DME and CO were introduced into the reactor from the top of the first catalyst bed layer, but H$_2$ was introduced into the second catalyst bed layer directly through an inner stainless steel tube equipped with evenly distributed holes. Benefitting from the precise control of the distribution of the reactants on the surface of different catalysts, an enhanced catalytic performance was obtained compared with the conventional dual bed reactor which introduced DME and syngas into the reactor simultaneously. The synergistic effects offered by this novel dual bed reactor were further confirmed by numerous comparative tests. Our results show that the excellent catalytic performance in this novel dual bed reactor was ascribed to the improved CO partial pressure in the upper zeolite catalyst bed. Compared with the conventional dual bed reactor, both DME conversion and EtOH yield were almost doubled in this novel dual bed reactor packed with the combination of H-Ferrierite and CuZnAl catalyst.

## 1. Introduction

Ethanol (EtOH), a basic chemical product, has been widely used as solvent, industrial intermediate and promising fuel additive. For industrial EtOH production, sugar fermentation and ethylene hydration are major synthesis routes.[1–3] However, sugar fermentation may aggravate the food crisis and face the problem of high cost due to the high energy demand to isolate the products. And the ethylene hydration strategy also is constrained with the diminishing of crude oil, as ethylene is mostly produced by the cracking of petroleum derivatives. Therefore, it is necessary to develop new EtOH synthesis routes from non-edible biomass or other fossil resources.[4–7] At present, some potential routes for EtOH synthesis have been widely investigated, such as the direct synthesis of EtOH from syngas (CO + H$_2$) over Rh-based catalysts, production of EtOH from syngas with dimethyl oxalate (DMO) as the intermediate using Cu-based catalysts, and methanol (MeOH) homologation

process with the combination of transition-metal catalysts and iodine compounds as promoters.[1,3,6,8–10] But the commercial applications of the above mentioned strategies are hampered by the usage of noble metal catalysts, tedious process, and lower selectivity of EtOH.

Recently, Iglesia and co-workers reported that H-Modernite (MOR) and H-Ferrierite (FER) zeolites are selective catalysts for dimethyl ether (DME) carbonylation at low temperature from 423 to 463 K, which provide a promising non-haldide and noble metal-free route to produce methyl acetate (MA).[11–13] A common feature of MOR and FER is the existence of 8-member ring channels, where the DME carbonylation reaction mainly occurs.[14–23] Considering that the DME carbonylation to MA and ester hydrogenation to alcohols occured at a similar temperature, a novel process for direct synthesis of EtOH from DME and syngas using a dual-bed reactor has been proposed by our group.[24–29] Briefly, the DME was firstly converted to MA through carbonylation on a solid acid zeolite catalyst such as MOR or FER in the first stage of the reactor, and then the formed MA was hydrogenated to EtOH on a Cu-based catalyst in the second stage of the reactor. These two reactions at different stages can be described as follows:

$$CO + CH_3OCH_3 \rightarrow CH_3COOCH_3 \qquad (1)$$

$$CH_3COOCH_3 + 2H_2 \rightarrow CH_3CH_2OH + CH_3OH \qquad (2)$$
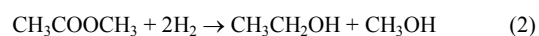
[a.] State Key Laboratory of High-efficiency Utilization of Coal and Green Chemical Engineering, Ningxia University, Yinchuan 750021, PR China
[b.] Department of Applied Chemistry, School of Engineering, University of Toyama, Gofuku 3190, Toyama 930-8555, Japan. E-mail: tsubaki@eng.u-toyama.ac.jp; Tel.: +81 76 4456846; Fax: +81 76 4456846
[c.] Key Laboratory of Mesoscopic Chemistry of MOE, Jiangsu Key Laboratory of Vehicle Emissions Control, Jiangsu Provincial Key Laboratory of Nanotechnology, School of Chemistry and Chemical Engineering, Nanjing University, Nanjing 210093, PR China
[d.] HighChem Company, Ltd., 8F Sakurabashi No.3 Bldg. 4-7-1 Hachobori, Chuo-Ku, Tokyo 104-0032, Japan

ARTICLE

The main byproduct of this process is MeOH, which can be recycled to synthesize DME over other solid acid catalysts through catalytic dehydration.[30]

In the conventional dual bed system (Scheme 1a), the DME and syngas are introduced into the reactor simultaneously. Nevertheless, it's no doubt that the carbonylation of DME with
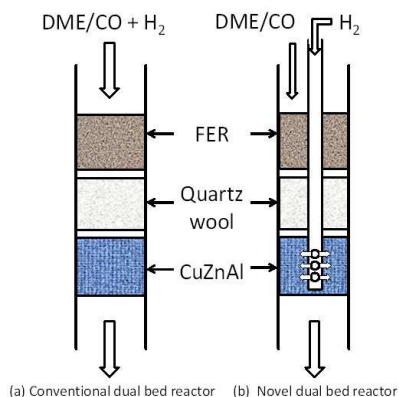
Scheme 1 Illustration of the (a) conventional dual bed reactor and (b) novel dual bed reactor, and the varied importing ways of feed gas: (a) DME/CO and H₂ were introduced simultaneously from the reactor inlet; (b) DME/CO and H₂ were respectively introduced to the top catalyst layer and the bottom catalyst layer in the reactor.

CO will be suppressed due to the lower accessibility of DME and CO caused by the co-feed of H_2.[26, 29] Wang et al. also found that the presence of H_2 in the first stage of the reactor decreased DME conversion and MA selectivity by suppressing the CO reaction with the intermediate methyl.[22] As the DME conversion rate is proportional to the partial pressure of $CO^{[11]}$, improving the partial pressure of CO in the first stage will be helpful to increase the conversion of DME and facilitate the EtOH formation in the second stage of the reactor.

Herein, a novel dual bed reactor is designed and employed for the highly efficient synthesis of EtOH from DME, CO and H_2 in a one-pot process. As shown in Scheme 1b, the DME and CO are routinely introduced to the upper zeolite (MOR or FER) bed to drive the carbonylation reaction, and the H_2 is directly introduced into the second CuZnAl catalyst bed through an inner stainless steel tube equipped with evenly distributed holes. As a result, the CO partial pressure at the upper zeolite layer of this novel dual bed reactor was improved nearly 100% than that of the conventional dual bed reactor. Surprisingly, due to this smart strategy, the DME conversion and EtOH yield were significantly enhanced compared with the conventional dual bed reactor.

2. Experimental

2.1 Catalyst Preparation.

H-type MOR zeolite (SiO₂/Al₂O₃ = 18) and H-type FER zeolite (SiO₂/Al₂O₃ = 18) were purchased from Tosoh Corporation for DME carbonylation. Prior to the reaction, the zeolite sample

was calcined in air at 823 K for 3 h, and then granulated into the size of 20–40 mesh.

The CuZnAl (molar ratio of Cu/Zn/Al = 1:1:0.1) catalyst was prepared by a homogeneous precipitation method as our previous work.[29] Briefly, aqueous solution of Cu(NO₃)₂·3H₂O, Zn(NO₃)₂·6H₂O and Al(NO₃)₃·9H₂O were added to the aqueous solution of urea with constant stirring. The mixing solution was heated to 363 K and maintained at this temperature for 2 h until the mixture were completely precipitated. The obtained slurry was aged overnight at ambient temperature, and then filtrated and washed with deionized water. After drying at 393 K and calcination in air at 623 K for 2 h, the sample was also granulated into the size of 20–40 mesh.

The obtained zeolite catalyst and CuZnAl catalyst were respectively loaded as the top and bottom catalysts layer in one reactor, as shown in Scheme 1. Prior to reaction, the CuZnAl catalyst was reduced in situ in a pure hydrogen flow at 573 K for 10 h.

2.2 Catalyst characterization.

The textural property of the catalyst was determined by N_2 physisorption instrument (Quantachrome Nova 2200e). The crystalline phase of the catalyst was measured by a Rigaku UltimaIV X-ray diffractometer with a Cu K_α radiation (λ= 0.154 nm) at 40 kV and 30 mA. The surface morphology of catalyst was observed using a JEOL JSM-6360LV scanning electron microscope (SEM). The elemental composition of the catalyst was measured by a JED-2300 energy dispersive spectrometer (EDS) equipped on SEM apparatus.

2.3 Catalytic reaction

2.3.1 EtOH synthesis reaction. The EtOH synthesis reaction was carried out in a novel dual bed stainless steel reactor (9.5 mm OD) as shown in Scheme 1b. Typically, 0.5 g MOR or FER zeolite catalyst was loaded at the first stage of the reactor, and another 0.5 g CuZnAl catalyst was loaded at the second stage of the reactor. For the separation of these two catalysts, the quartz wool was loaded between them. A gas mixture of Ar/DME/CO (molar ratio of 3/4/93 with a flow rate of 20 mL/min) was firstly introduced into the reactor from the inlet of the reactor, and the pure H_2 (flow rate of 20 mL/min) was directly introduced into the second stage of the dual bed reactor through an inner stainless steel tube equipped with evenly distributed holes (0.5 mm in diameter). Prior to the EtOH synthesis reaction, the catalysts were reduced in situ in a pure hydrogen flow at 573 K and atmospheric pressure for 10 h. The reaction was initiated after the reactor temperature cooled down to 493 K and the pressure increased to 1.5 MPa.

As reference, the EtOH synthesis reaction was also studied in a conventional dual bed reactor, as shown in Scheme 1a. The reaction pressure and temperature were the same to those of the novel dual bed reactor; however, the reactant gases Ar/DME/CO and H_2 were simultaneously introduced into the reactor from the inlet of the reactor. Comparatively, the EtOH synthesis reaction was also performed in the novel dual

bed reactor with H_2 introduced into the different locations of this novel reactor, such as into inlet, zeolite bed, quartz wool, CuZnAl catalyst bed, or outlet layer of the reactor. The DME conversion was calculated after the reaction reached stable state (at TOS = 10 h), and the product selectivities were collected and calculated by the data from 8 to 10 h.

2.3.2 DME carbonylation reaction. In order to compare the catalytic performance of these two zeolite catalysts (MOR and FER) in the DME carbonylation reaction, the single DME carbonylation reaction was also performed in these two types of reactors with only zeolite catalyst.

To study the effect of H_2 on the carbonylation reaction, the DME carbonylation was carried out over FER catalyst in the conventional dual bed reactor with different H_2 compositions. The gas mixture of Ar/DME/CO (molar ratio of 3/4/93) was kept in a flow rate of 20 mL/min, while the H_2 flow rate was systematically increased from 0, 5, 10, 15 to 20 mL/min.

To further clarify the relationship of DME conversion with the reaction pressure, the DME carbonylation was evaluated with the feeding stream of Ar/DME/CO (molar ratio of 3/4/93) over the FER catalyst under different reaction pressures.

After reaction, the released effluent gases passed through an ice trap firstly, and then were analyzed by an online gas chromatographs (GC). The CO, CO_2, CH_4 and Ar (Ar was employed as the internal standard) were analyzed by a Shimadzu GC-8A with a thermal conductivity detector (TCD) and an activated carbon column; DME was analyzed by the TCD with another Porapak Q column. The liquid products MA, MeOH, EtOH and ethyl acetate (EA) collected by the ice trap with 1-butanol as solvent were analyzed by another Shimadzu GC-8A with a flame-ionization detector (FID) and a connected dual column packed by Gaskuropack 54 and Porapak N packing materials. Before analysis, 1-propanol was added into the liquid products as the internal standard. The DME conversion (X_{DME}) was calculated by internal standard method, and the selectivity values of the products (S_i) were calculated in molecular selectivity. The EtOH yield (Y_{EtOH}) was calculated with the DME conversion and EtOH selectivity using following formulas:

$$X_{DME} (\%) = (X_{DME,in}/Ar_{in} - X_{DME,out}/Ar_{out}) / (X_{DME,in}/Ar_{in}) \times 100\%$$

$$S_i (\%) = n_i/\Sigma n_i \times 100\% \ (i = MA, MeOH, EtOH, EA, CO_2, CH_4)$$

$$Y_{EtOH} (\%) = X_{DME} \times S_{EtOH}$$

3. Results and discussion

3.1 Catalyst characterization

3.1.1 X-ray diffraction (XRD) and N_2-adsorption results. The XRD patterns of the MOR zeolite, FER zeolite and CuZnAl catalyst are presented in Fig. 1. Both MOR and FER zeolites exhibit typical diffraction peaks of their unique crystal structures.[19, 20, 23, 29] For the CuZnAl catalyst, the diffraction peaks appearing at 2θ = 31.8°, 34.4°, 36.3°, 47.5°, 56.6°, 62.9° and 68.0° are

assigned to ZnO, and the diffraction peaks appearing at 2θ = 35.5°and 38.7° are assigned to CuO.[27, 29] On the basis of the Scherrer formula, the average crystallite size of the CuO particles over CuZnAl catalyst is about 15.7 nm.
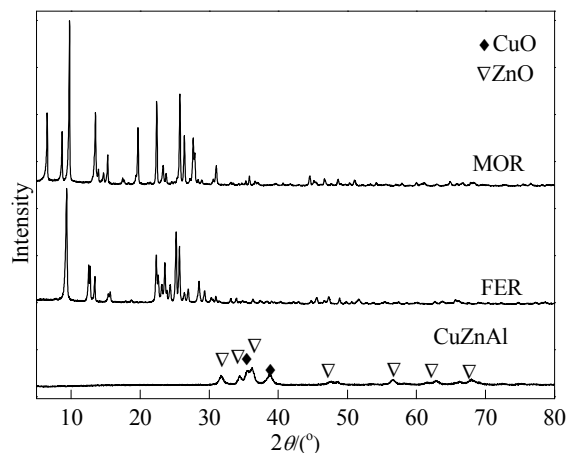

Fig. 1 The XRD patterns of the MOR, FER and CuZnAl catalyst.

The BET specific surface area, pore volume and average pore diameter of the catalysts were measured by N_2 physisorption and summarized in Table l. The MOR catalyst shows larger specific surface area than that of FER, however, the pore volume and average pore diameter are almost same. The CuZnAl catalyst possesses a specific surface area of 47 m^2 g^{-1}.

N_2 adsorption-desorption isotherms and relevant pore size distribution results of catalysts are depicted in Fig. 2. Both MOR and FER showed a combination of type I and IV isotherms with hysteresis loops (from 0.1 to 0.9 P/P^0 in Fig. 2a, from 0.2 to 0.9 P/P^0 in Fig. 2b), indicating the existence of both micro- and mesopores. As reported, the DME carbonylation reaction mainly occurs within the micropores.[12] Those mesopores existed among MOR and FER are favorable for the reactants and products transportation. In Fig. 2c, a typical mesopore structure was detected on CuZnAl catalyst, which showed a type IV isotherm with hysteresis loop beginning at a P/P^0 value of 0.8. The micropores size distribution of MOR and FER are shown in Fig. 2a (inset) and Fig. 2b (inset), respectively. Two micropores at around 0.53 nm and 0.57 nm were detected over MOR zeolite, while only one micropore at around 0.54 nm was observed over FER zeolite. For CuZnAl (Fig. 2c), the pore size mainly distributed around 22 nm.

Table 1 The physical properties of different catalysts.

Catalysts	Specific surface areas (m^2 g^{-1})	Average pore diameter (nm)	Pore Volume[a] (mL g^{-1})	SiO_2/Al_2O_3 molar ratio[b]
MOR	446	2.5	0.3	13
FER	297	4.1	0.3	13
CuZnAl	47	8.7	0.2	-

[a] Characterized using the N_2 adsorption method.

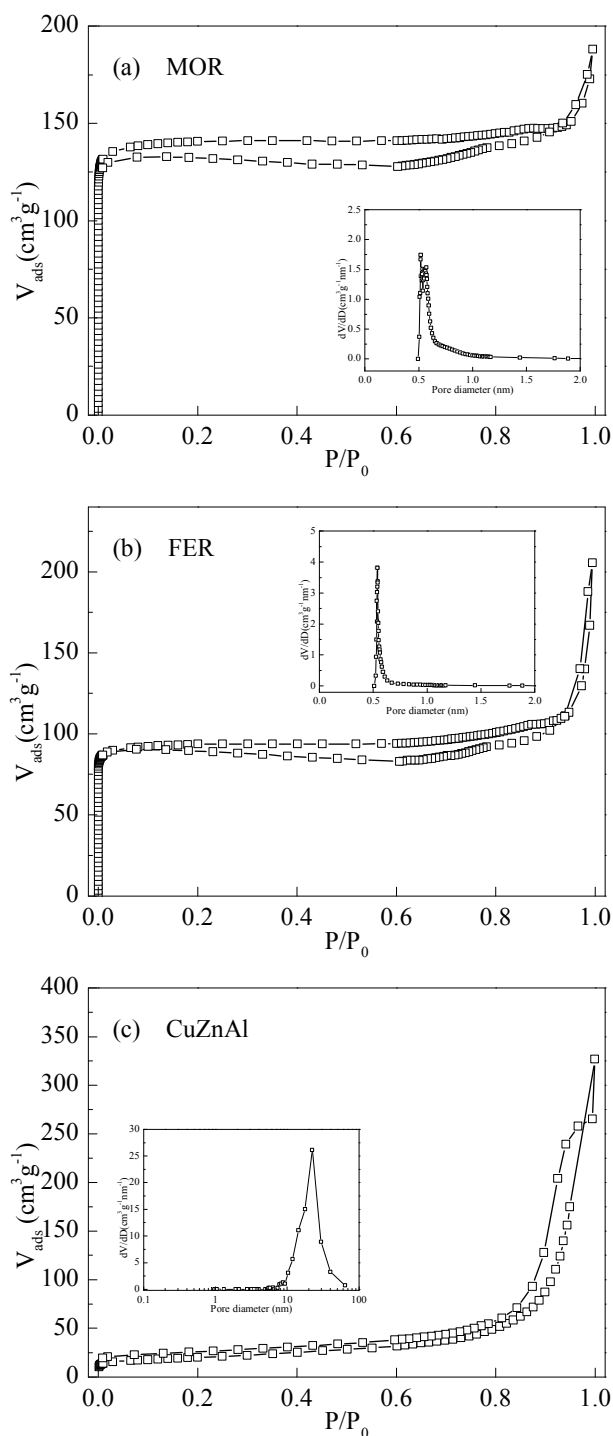[b] Calculated from EDS analysis.

ARTICLE

Fig. 2 N_2 adsorption isotherms and pore size distribution curves (inset) of catalysts: MOR (a), FER (b), and CuZnAl (c).

3.1.2 SEM-EDS analysis. Fig. 3 displays SEM images and EDS results of MOR and FER catalyst. Both MOR (Fig. 3a) and FER (Fig. 3c) exhibit a traditional block-like morphology. They comprised the aggregation of nanoparticles, where mesopores were formed between these adjacent nanoparticles. It is in accordance with the N_2-adsorption results of hysteresis loops
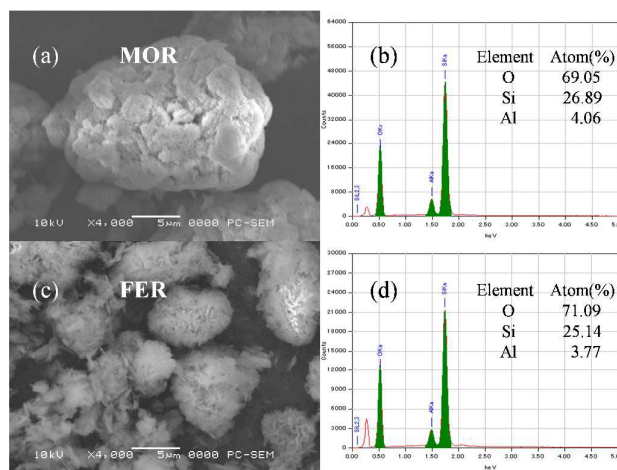

Fig. 3 SEM images and EDS analyses of catalysts: MOR (a) and (b), FER (c) and (d).

detected on MOR and FER catalyst. EDS (Fig. 3b and d) was used to quantify the element composition of catalysts. Both MOR and FER show the SiO_2/Al_2O_3 molar ratio of 13 (Table 1).

3.2 DME carbonylation in different reactors over pure MOR or FER catalyst

At first, the catalytic performance of the MOR catalyst for the DME carbonylation reaction was studied in the conventional dual bed reactor and the novel dual bed reactor, respectively. The reaction results are shown in Fig. 4 and Table 2. In these cases, the CuZnAl catalyst was not loaded into the reactor. The DME conversion over MOR catalyst in the novel dual bed reactor was nearly doubled if compared to that of the conventional dual bed reactor, while keeping the same MA selectivity. However, MOR catalyst exhibits poor stability during the reaction, the DME conversion decreased slightly after 2.5 h time on stream. This is probably due to the high acid density of 12-member ring channel in MOR, which will lead to catalyst deactivation by coke deposition.[14–16] In contrast, FER zeolite consists of a one-dimensional channel of 8-member ring and a perpendicularly intersected one-dimensional channel of 10-member ring, which can reduce the hydrocarbon depositions by restricting the diffusion of reactants due to the steric hindrance effects of 10-member ring channels.[17, 18] Thus, FER zeolite was then employed as the DME carbonylation catalyst in both types of reactors. In Fig. 4b, the DME conversion over the FER in the novel dual bed reactor was also about doubled, over that in the conventional dual bed reactor. The MA selectivities in these two reactors were both higher than 94% (see Table 2). After 4 h time on stream, the DME conversion was increased. In comparison with MOR, the FER catalyst exhibited superior stability for the DME carbonylation reaction.
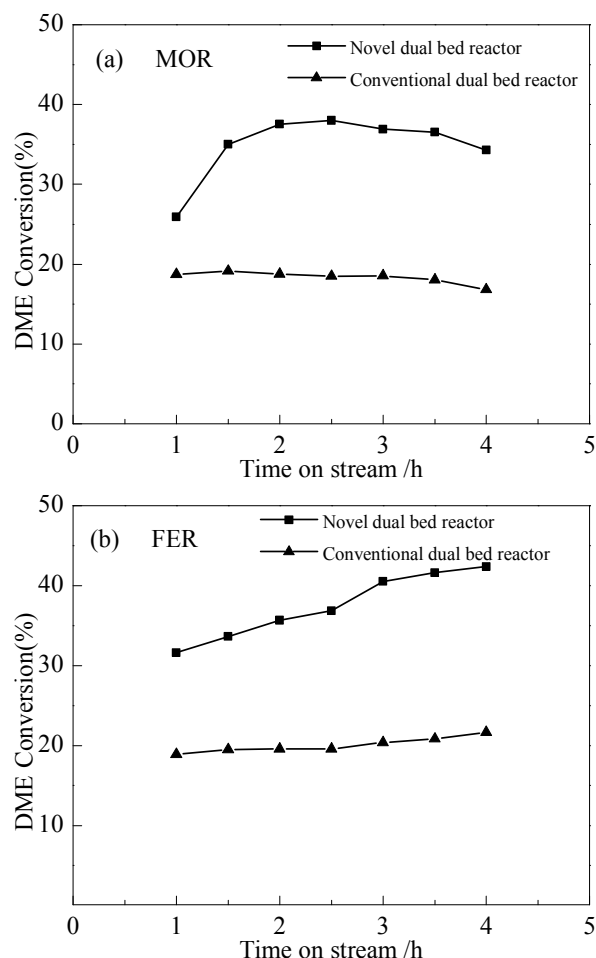
Journal Name

ARTICLE

Fig. 4 Catalytic performance tests of (a) MOR and (b) FER catalysts for DME carbonylation reaction in the conventional dual bed and novel dual bed reactor. Reaction conditions: 493 K, 1.5 MPa, 0.5 g MOR or FER, Ar/DME/CO = 3/4/93 (20 mL/min), 100% H_2 (20 mL/min).

Both MOR and FER catalysts realized significantly enhanced catalytic activity in the novel dual bed reactor, compared with those in the conventional dual bed reactor. This result could be attributed to the higher CO partial pressure in the reactor without co-feed of H_2.[22] In conventional dual bed reactor, the

Table 2 DME carbonylation in the conventional dual bed reactor and novel dual bed reactor over MOR or FER catalysts.

Catalysts	Selectivity (%)		
	MA	MeOH	CH_4
MOR[a]	95.63	3.71	0.66
MOR[b]	96.37	3.18	0.45
FER[a]	94.71	4.68	0.61
FER[b]	95.28	4.15	0.57

[a] Conventional dual bed reactor; [b] Novel dual bed reactor.

Reaction conditions: 493 K, 1.5 MPa, 0.5 g cat., Ar/DME/CO = 3/4/93 (20 mL/min), 100% H_2 (20 mL/min).

20 mL/min Ar/DME/CO (Ar/DME/CO in a molar ratio of 3/4/93) was mixed with another 20 mL/min pure H_2 in the inlet of the reactor. For the reason that the total pressure was 1.5 MPa, the CO partial pressure in the zeolite layer was only 0.7 MPa. However, in the novel reactor, the H_2 was directly introduced into the second CuZnAl stage of the reactor, below the zeolite layer in the first stage. The CO partial pressure in the zeolite layer should be as high as 1.4 MPa in theory, where the H_2 gas could not enter the zeolite layer. To verify the influence of the accompanying H_2 gas on the DME carbonylation, the DME carbonylation reaction with different H_2 contents in the raw materials was studied as follows.

3.3 Effect of H_2 presence on DME carbonylation reaction

In the conventional dual bed reactor, H_2 firstly passed through the upper zeolite layer, and then entered into the following Cu-based catalyst layer for EtOH synthesis. It is necessary to investigate the effect of H_2 on DME carbonylation at the upper layer. In this part, the DME carbonylation with different H_2 flow rates was carried out over FER catalyst in the conventional dual bed reactor, and the reaction results are shown in Fig. 5. The flow rate of the mixture gas Ar/DME/CO (3/4/93) was kept at 20 mL/min for all experiments while the H_2 flow rate was gradually increased. When the H_2 flow rate increased from 0 to 20 mL/min, the DME conversion gradually decreased from 40% to 20%, which should be caused by the decrease of the CO partial pressure in the zeolite layer.[26, 29] It is noteworthy that the DME conversion obtained from the conventional dual bed reactor without H_2 was about 40%, similar to that of the novel dual bed with H_2 flow rate of 20 mL/min in the feed gas, as shown in Fig. 4b. It also indicates that the novel dual bed reactor with single zeolite catalyst layer could be assumed as a plug flow model reactor, without H_2 back-mixing. In addition, the effects of possible H_2 adsorption on the active zeolite acid sites to the simultaneous
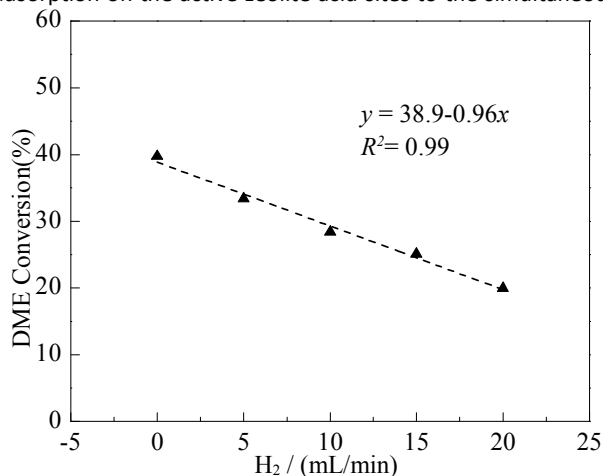

$y = 38.9 - 0.96x$

$R^2 = 0.99$

Fig. 5 Effect of H_2 composition in feed gas on DME conversion over FER catalyst. Reaction conditions: 493 K, 1.5 MPa, 0.5g FER, Ar/DME/CO = 3/4/93 (20 mL/min), 100% H_2 (0, 5, 10, 15, 20 mL/min).
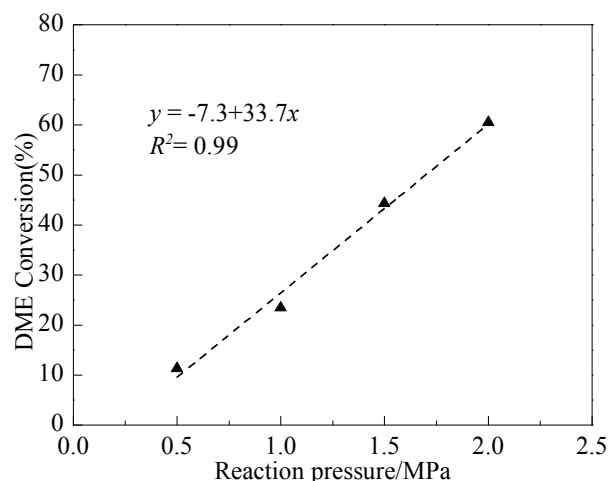
Fig. 6 Effect of the reaction pressure on DME conversion over FER catalyst. Reaction conditions: 493 K, 0.5 g FER, Ar/DME/CO = 3/4/93 (20 mL/min), Reaction pressure (0.5, 1.0, 1.5, 2.0 MPa).

adsorption of DME on the same active sites could be erased in the novel dual bed reactor.

3.4 Effect of reaction pressure on DME carbonylation reaction

In order to confirm the relationship between DME conversion and reaction pressure, the DME carbonylation reaction using single FER catalyst was investigated in the conventional dual bed reactor under different pressures. As shows in Fig. 6, the DME conversion is almost proportional to reaction pressure (0.5–2.0 MPa). The DME conversions are 18 and 43% at reaction pressure of 0.75 and 1.5 MPa, respectively. This result shows that the differences of DME conversion in the conventional and novel dual bed reactor were caused by the different CO partial pressure. Iglesia and co-workers found that the rate of MA synthesis did not depend on DME pressure, however, was proportional to CO pressure.[11] Therefore, the kinetically relevant steps involve reactions of gas-phase or adsorbed CO with DME-derived intermediates.[11] This result indicates that increasing CO partial pressure in the zeolite bed layer will be beneficial for DME conversion.

3.5 EtOH synthesis with the combination of FER and CuZnAl catalyst

Fig. 7 shows the comparison results of the DME conversions and product selectivities over the combination of FER and CuZnAl catalyst in the conventional dual bed reactor and the novel dual bed reactor. The DME conversions (Fig. 7a) at 15 h were 23% in the conventional and 42% in the novel dual bed reactor, respectively. This could be explained by the different CO partial pressures in the first stage of these two reactors. Similar product selectivity values were obtained in these two types of reactors, and the results are presented in Fig. 7b and c. The main products are EtOH and MeOH, which are formed by the MA hydrogenation over the CuZnAl catalyst.

The EtOH yield was calculated with the DME conversion and EtOH selectivity. The EtOH yields at 15 h were 19% in the novel dual bed reactor and 10% in the conventional dual bed reactor. The EtOH yield in this novel dual bed reactor was almost twice
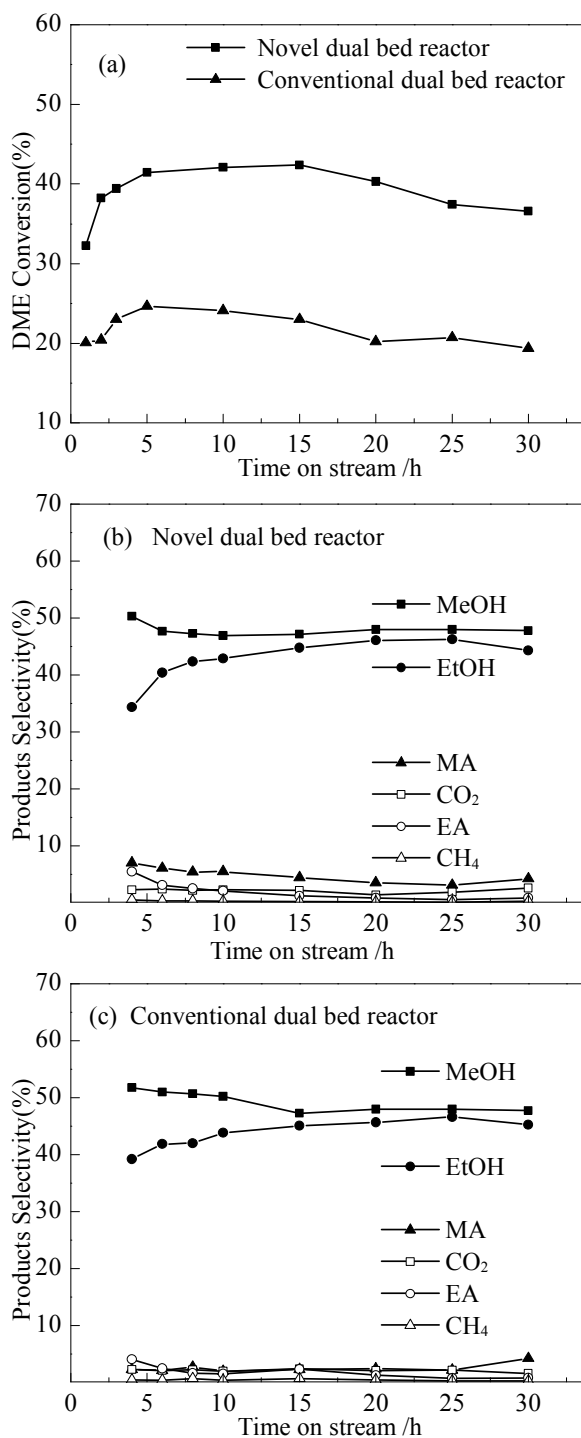
Fig. 7 EtOH synthesis in the novel dual bed reactor and the conventional dual bed reactor over the combination of FER and CuZnAl catalyst. (a)DME conversions in two reactors; (b) Products selectivities in the novel dual bed reactor and (c) conventional dual bed reactor. Reaction conditions: 493 K, 1.5 MPa, 0.5 g FER, 0.5 g CuZnAl, Ar/DME/CO = 3/4/93 (20 mL/min), 100% H$_2$ (20 mL/min).

as high as that from the conventional dual bed reactor. Compared with previous works using the conventional dual bed reactor (Table 3), the highest EtOH yield (19%) was obtained in this work. This value is also competitive to the one

Table 3 Comparison with previous results in the one-step EtOH synthesis.

Catalysts	Gas composition	Reactor type	Time on stream (h)	DME Conversion	EtOH Selectivity	EtOH Yield	Reference
HMOR-Cu/SBA-15[a]	N_2/DME/CO/H_2 = 6.25/1.56/29.69/62.50	Two-stage	6	72.1%	37.8%	27.3%	[22]
MOR-Cu/ZnO[b]	Ar/DME/CO/H_2 = 1.42/2.83/45.75/50	Conventional dual bed	2	49.7%	37%	18.4%	[27]
Pt/MOR-Cu/ZnO[b]	Ar/DME/CO/H_2 = 1.55/2.35/46.1/50	Conventional dual bed	2	35.2%	32.6%	11.5%	[28]
Cu-HZSM-35-Cu/Zn/Al[b]	Ar/DME/CO/H_2 = 1.51/2/46.49/50	Conventional dual bed	4	27.1%	46.7%	12.7%	[29]
FER-CuZnAl[b]	Ar/DME/CO/H_2 = 1.5/2/46.5/50	Novel dual bed	30	42%	45%	19%	Present work

[a]The mixture flow of DME and CO (n(CO)/n(DME) = 19): 15 mL/min, Carbonylation: 483 K, Hydrogenation: 503 K, 1.8 MPa, 0.5g HMOR, 2.0g Cu/SBA-15.

[b]Feed gas flow rate = 40 mL/min, 493 K, 1.5 MPa, Zeolite = 0.5 g, Cu-based catalyst = 0.5 g.

obtained using a two-stage type reactor with the connected two reactors (Table 3). Furthermore, the combination of FER and CuZnAl catalyst exhibits a good stability in the EtOH synthesis reaction. Our new catalyst here was stable for about 30 h time on stream, whereas the catalysts in previous reports deactivated rapidly within 4 h.[27–29]

3.6 EtOH synthesis in novel dual bed reactor with different introduced locations of H_2

To study the effect of H_2 introduced locations on the EtOH synthesis reaction, this reaction was carried out over FER and CuZnAl catalysts in the novel dual bed reactor. H_2 was introduced into the reactor from the inlet, FER bed, quartz wool, CuZnAl catalyst bed, or outlet layer stage of the reactor respectively. With the H_2 introduced location shifting from the inlet to the CuZnAl catalyst bed of the reactor stepwise, the DME conversion increases from about 23% to 41% (Fig. 8). Except being located at outlet layer, the selectivities of MeOH and EtOH are almost the same as in Table 4. The EtOH yield increases in this novel dual bed reactor, which can be ascribed to the high efficiency in the DME carbonylation process. However, when the H_2 was introduced directly into the outlet of the reactor, the main product was MA. Thereby, it is obvious that the CuZnAl catalyst plays the key role for converting MA to EtOH in the second stage.

It is noteworthy that the DME conversion in the case of H_2 gas being introduced at the quartz wool layer location is not twice as high as that at the inlet layer, and also not the same to that at the CuZnAl catalyst layer. This result indicates that the back-mixing of H_2 existed to some extent in this system, which may be caused by the quartz wool layer. However, when the H_2 introduced location shifted to CuZnAl catalyst layer, the back-mixing of H_2 was sufficiently suppressed, ensuring the excellent catalytic performance of this novel dual bed reactor.

Table 4 EtOH synthesis in the novel dual bed reactor with different H_2 imported locations over the combination of FER and CuZnAl catalysts.

H_2 imported locations	Selectivity (%)					
	MeOH	EtOH	MA	EA	CO_2	CH_4
Inlet	47.81	47.12	2.13	0.74	1.71	0.49
FER	48.24	46.27	2.28	0.72	1.86	0.63
Quartz wool	46.32	45.74	3.65	1.61	2.12	0.56
CuZnAl	46.41	45.05	3.94	1.85	2.14	0.61
Outlet	7.02	2.31	90.02	0	0.08	0.57

Reaction conditions: 493 K, 1.5 MPa, 0.5 g FER, 0.5 g CuZnAl, Ar/DME/CO = 3/4/93 (20 mL/min), 100% H_2 (20 mL/min).
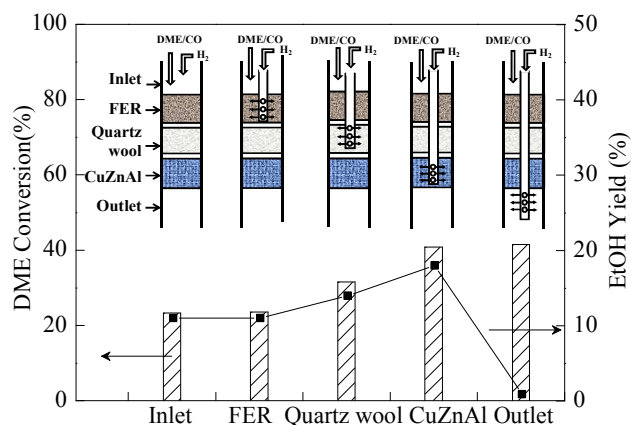
Fig. 8 EtOH synthesis in the novel dual bed reactor with different H_2 imported locations over the combination of FER and CuZnAl catalyst. Reaction conditions: 493 K, 1.5 MPa, 0.5 g FER, 0.5 g CuZnAl, Ar/DME/CO = 3/4/93 (20 mL/min), 100% H_2 (20 mL/min).

3.7 Numerical analysis of gas flow in novel dual bed reactor

On the basis of the above experiment results, the back-mixing of H_2 into the first stage could be prevented when the H_2 was directly introduced to the second stage of the reactor. Herein, the nature of gas flow in this novel dual bed reactor was

ARTICLE

Journal Name

discussed numerically. Generally, the Reynolds number is used to determine whether the flow of a fluid is laminar or turbulent.[31–33] In this part, we analyzed the flow type of the fluid in the first and second stage of the reactor, respectively.

To simplify calculations, the feed gas in the first stage of the reactor is assumed as 100% CO, because of very high content of CO gas in this stage (Ar/DME/CO = 3/4/93). At the second stage, even though the DME has been converted 41%, its influence still can be ignored in our calculations, owing to the low content of DME gas in the system. Therefore, the feed gas in the second stage is assumed as a mixture of 50% CO and 50% H_2. The parameters of the catalysts, the reactor and the Reynolds number values are listed in Table 5. Their symbols are also defined in Table 5.

The Reynolds number in the two stages of the novel dual bed reactor could be calculated as follows:[31–33]

$$R_{eM} = \frac{d_p \rho_f u_f}{\mu}\left(\frac{1}{1-\varepsilon_{BM}}\right) = \frac{d_p G}{\mu}\left(\frac{1}{1-\varepsilon_{BM}}\right) \qquad (1)$$

In the above equation, d_p, ρ_f, u_f, μ, and ε_{BM} could be calculated as follows:

Geometric average diameter d_p of catalyst particles is:

$$d_p = \sqrt{d_{pr1} \times d_{pr2}} = \sqrt{3.8\times10^{-4}\times8.3\times10^{-4}} = 5.6\times10^{-4} \quad (2)$$

Density ρ_f of gas flow at 493 K, 1.5 MPa was calculated based on ρ_{fs} at standard temperature (273 K) and pressure (0.1 MPa) with the ideal gas law of $PV=nRT$,

$$\rho_{f1} = \frac{P/T}{P_s/T_s} \times \rho_{fs1} \qquad (3)$$

$$\rho_{f1} = \frac{P/T}{P_s/T_s} \times \rho_{fs1} = \frac{1.5/493}{0.1/273}\times1.25 = 10.38$$

$$\rho_{f2} = 0.74$$

$$\rho_{fm} = \frac{\rho_{f1} + \rho_{f2}}{2} = 5.56$$

Superficial velocity u_f of gas is:

$$u_f = \frac{G}{\rho_f} \qquad (4)$$

where the mass flow rate G of the gas is:

$$G = \frac{\rho_{fs} \times u_{fs}}{A} \qquad (5)$$

$$G_1 = \frac{\rho_{fs1} \times u_{fs1}}{A} = \frac{1.25\times3.3\times10^{-7}}{4\times10^{-5}} = 1.0\times10^{-2}$$

$$G_m = \frac{\rho_{fsm} \times u_{fsm}}{A} = \frac{0.67\times6.6\times10^{-7}}{4\times10^{-5}} = 1.1\times10^{-2}$$

in which, the cross sectional area A of reactor is:

$$A = \pi\left(\frac{d_r}{2}\right)^2 - \pi\left(\frac{d_o}{2}\right)^2 = \pi\left(\frac{7.5\times10^{-3}}{2}\right)^2 - \pi\left(\frac{2.5\times10^{-3}}{2}\right)^2 = 4\times10^{-5} \qquad (6)$$

$$u_{f1} = \frac{G_1}{\rho_{f1}} = \frac{1.0\times10^{-2}}{10.38} = 9.6\times10^{-4}$$

$$u_{fm} = \frac{G_m}{\rho_{fm}} = \frac{1.1\times10^{-2}}{5.56} = 1.98\times10^{-3}$$

The viscosities of CO and H_2 at 493 K were listed in Table 5, and the viscosity μ_m of the mixture of H_2 and CO could be calculated as follows:[34]

$$\mu_m = \frac{\sum_{i=1}^{n}\mu_i x_i\sqrt{M_i}}{\sum_{i=1}^{n}x_i\sqrt{M_i}} = \frac{2.56\times10^{-5}\times50\%\sqrt{28} + 1.23\times10^{-5}\times50\%\sqrt{2}}{50\%\sqrt{28} + 50\%\sqrt{2}} = 2.28\times10^{-5} \qquad (7)$$

Equation (8), (9) and (10) were used to calculate the void fraction:[35]

$$\varepsilon_B = 0.38 + 0.073\left[1 + \frac{\left(\frac{d_t}{d_p} - 2\right)^2}{\left(\frac{d_t}{d_p}\right)^2}\right] \qquad (8)$$

where the equivalent diameter of the reactor d_t could be calculated from:

$$\pi\left(\frac{d_t}{2}\right)^2 = \pi\left(\frac{d_r}{2}\right)^2 - \pi\left(\frac{d_o}{2}\right)^2 \qquad (9)$$

$$\pi \left(\frac{d_t}{2}\right)^2 = \pi \left(\frac{7.5 \times 10^{-3}}{2}\right)^2 - \pi \left(\frac{2.5 \times 10^{-3}}{2}\right)^2$$

$$d_t = 7.1 \times 10^{-3}$$

$$\varepsilon_B = 0.38 + 0.073 \left[1 + \frac{\left(\frac{7.1 \times 10^{-3}}{5.6 \times 10^{-4}} - 2\right)^2}{\left(\frac{7.1 \times 10^{-3}}{5.6 \times 10^{-4}}\right)^2}\right] = 0.5$$

Considering the FER zeolite and CuZnAl catalysts are porous materials, calibration was performed on the ε_B as follows:

$$\varepsilon_{BM} = \left(V_b \times \varepsilon_B + V_p \times m\right)/V_b \tag{10}$$

$$\varepsilon_{BM1} = \frac{\left(V_{b1} \times \varepsilon_B + V_{p1} \times m\right)}{V_{b1}} = \frac{\left(1.2 \times 10^{-6} \times 0.5 + 3 \times 10^{-4} \times 5 \times 10^{-4}\right)}{1.2 \times 10^{-6}} = 0.63$$

$$\varepsilon_{BM1} = \left(V_{b1} \times \varepsilon_B + V_{p1} \times m\right)/V_{b1} = \left(1.2 \times 10^{-6} \times 0.5 + 3 \times 10^{-4} \times 5 \times 10^{-4}\right)/1.2 \times 10^{-6} = 0.63$$

$$\varepsilon_{BM2} = \left(V_{b2} \times \varepsilon_B + V_{p2} \times m\right)/V_{b2} = \left(6 \times 10^{-7} \times 0.5 + 2 \times 10^{-4} \times 5 \times 10^{-4}\right)/6 \times 10^{-7} = 0.67$$

The void fractions of the first and second stage of the reactor are $\varepsilon_{BM1} = 0.63$ and $\varepsilon_{BM2} = 0.67$. The Reynolds numbers in these two stages of the reactor could be calculated following the above equations, in which $R_{eM1} = 0.59$ and $R_{eM2} = 0.82$. Both Reynolds number values in these two stages are less than 10, which should be considered to be laminar flow (fluid flow through a packed bed is considered to be laminar if the Reynolds number is less than 10).[31–33]

The pressure drops through the first and second stage of the catalyst bed were calculated with Ergun equation, as follows:

$$\frac{\Delta p}{L} = 150 \frac{(1-\varepsilon_{BM})^2}{\varepsilon_{BM}^3} \frac{\mu_m \, u_f}{d_p^2} + 1.75 \frac{1-\varepsilon_{BM}}{\varepsilon_{BM}^3} \frac{\rho_f \, u_f^2}{d_p} \tag{11}$$

$$\frac{\Delta p_1}{L_1} = 150 \frac{(1-\varepsilon_{BM1})^2}{\varepsilon_{BM1}^3} \frac{\mu_1 \, u_{f1}}{d_p^2} + 1.75 \frac{1-\varepsilon_{BM1}}{\varepsilon_{BM1}^3} \frac{\rho_{f1} \, u_{f1}^2}{d_p}$$

$$= 150 \frac{\left(1-6.3 \times 10^{-1}\right)^2}{\left(6.3 \times 10^{-1}\right)^3} \frac{2.56 \times 10^{-5} \times 9.6 \times 10^{-4}}{\left(5.6 \times 10^{-4}\right)^2} + 1.75 \frac{1-6.3 \times 10^{-1}}{\left(6.3 \times 10^{-1}\right)^3} \frac{10.38 \times \left(9.6 \times 10^{-4}\right)^2}{5.6 \times 10^{-4}} = 6.48$$

$$\frac{\Delta p_2}{L_2} = 150 \frac{(1-\varepsilon_{BM2})^2}{\varepsilon_{BM2}^3} \frac{\mu_m \, u_{fm}}{d_p^2} + 1.75 \frac{1-\varepsilon_{BM2}}{\varepsilon_{BM2}^3} \frac{\rho_{fm} \, u_{fm}^2}{d_p}$$

$$= 150 \frac{\left(1-6.7 \times 10^{-1}\right)^2}{\left(6.7 \times 10^{-1}\right)^3} \frac{2.28 \times 10^{-5} \times 1.98 \times 10^{-3}}{\left(5.6 \times 10^{-4}\right)^2} + 1.75 \frac{1-6.7 \times 10^{-1}}{\left(6.7 \times 10^{-1}\right)^3} \frac{5.56 \times \left(1.98 \times 10^{-3}\right)^2}{5.6 \times 10^{-4}} = 7.89$$

The pressure drop through the first and second catalyst bed layer were 0.19 Pa and 0.12 Pa, respectively. The total pressure drop of these two catalyst beds was 0.31 Pa, which was insignificant to the operation pressure (1.5 MPa). The Ergun equation shows that the pressure drop through the reactor was proportional to the catalyst bed height. As a result, the system pressure in the first stage of the reactor was higher than that in the second stage.

Considering the laminar nature of the fluid flow and the higher pressure in the first stage of the reactor, the back-mixing of H_2 into the first stage could be ignored when the H_2 was directly introduced into the second stage of the reactor. Therefore, the partial pressure of CO in the first stage of the reactor was improved automatically. Furthermore, the DME conversion and EtOH yield were enhanced.

Conclusions

In this study, a novel dual bed reactor was successfully designed and employed as the catalytic reactor for EtOH synthesis via the sequential reactions of DME carbonylation and MA hydrogenation. Both MOR and FER zeolite catalysts showed high catalytic activity on DME carbonylation reaction. The DME conversion in this novel dual bed reactor was nearly doubled if compared with that in the conventional dual bed reactor. Moreover, the FER catalyst exhibited similar catalytic activity, but better stability than MOR catalyst in the DME carbonylation reaction. The effect of reaction pressure to the DME carbonylation using single FER catalyst was investigated in detail. The DME conversion was almost proportional to the reaction pressure. The numerical analysis result disclosed that

ARTICLE

Journal Name

the Reynolds numbers in this novel dual bed reactor were less than 10, which could be considered to be laminar flow. No back-mixing of H_2 was found, thus the partial pressure of CO in the upper zeolite bed of the novel dual bed reactor was around double higher than that of the conventional dual bed reactor. The DME conversion and EtOH yield were also doubled consequently. To the best of our knowledge, for the first time, this design concept of novel dual bed reactor was employed in EtOH synthesis from DME, CO, and H_2. Moreover, the optimal parameters for EtOH synthesis in this novel reactor were obtained. This smart design strategy can be also extended to other multistage sequential reactions.

Conflicts of interest

There are no conflicts to declare.

Table 5 Parameters of catalysts and reactor.

parameters	values	nomenclature	notes
d_{pr}(m)	$3.8 - 8.3 \times 10^{-4}$	diameter range of catalyst particles	20–40 mesh
d_p(m)	5.6×10^{-4}	geometric average diameter of catalyst particles	equation (2)
ρ_{fs1}(kg·m^{-3})	1.25	density of CO flow at 273 K, 0.1 MPa	
ρ_{fs2}(kg·m^{-3})	8.9×10^{-2}	density of H_2 flow at 273 K, 0.1 MPa	
ρ_{fsm}(kg·m^{-3})	0.67	density of the mixture of CO and H_2 at 273 K, 0.1 MPa	
u_{fs1}(m^3·s^{-1})	3.3×10^{-7}	flow rate of CO gas at 273 K, 0.1 MPa	
u_{fs2}(m^3·s^{-1})	3.3×10^{-7}	flow rate of H_2 gas at 273 K, 0.1 MPa	
u_{fsm}(m^3·s^{-1})	6.6×10^{-7}	flow rate of the mixture of CO and H_2 at 273 K, 0.1 MPa	
P(MPa)	1.5	operation pressure of fixed bed reactor	
T(K)	493	operation temperature	
ρ_{f1}(kg·m^{-3})	10.38	density of CO flow at 493 K, 1.5 MPa	equation (3)
ρ_{f2}(kg·m^{-3})	0.74	density of H_2 flow at 493 K, 1.5 MPa	equation (3)
ρ_{fm}(kg·m^{-3})	5.56	density of the mixture of CO and H_2 at 493 K, 1.5 MPa	
u_{f1}(m·s^{-1})	9.6×10^{-4}	superficial velocity of CO	equation (4)
u_{fm}(m·s^{-1})	1.98×10^{-3}	superficial velocity of the mixture of CO and H_2	equation (4)
G_1(kg·m^{-2}·s^{-1})	1.0×10^{-2}	mass flow rate of CO	equation (5)
G_m(kg·m^{-2}·s^{-1})	1.1×10^{-2}	mass flow rate of the mixture of CO and H_2	equation (5)
d_r(m)	7.5×10^{-3}	inner diameter of the reactor	
d_o(m)	2.5×10^{-3}	outer diameter of the inner pipe	
A(m^2)	4×10^{-5}	cross sectional area of reactor	equation (6)
μ_1(kg·m^{-1}·s^{-1})	2.56×10^{-5}	viscosity of CO at 493 K	reference [36]
μ_2(kg·m^{-1}·s^{-1})	1.23×10^{-5}	viscosity of H_2 at 493 K	reference [36]
x_i	50%	mole fraction of component i (CO or H_2)	
M_i(mol·g^{-1})	28(CO)/2(H_2)	molecular weight of component i	
μ_m(kg·m^{-1}·s^{-1})	2.28×10^{-5}	viscosity of the mixture of H_2 and CO at 493 K	equation (7)
ε_B	0.5	void fraction of fixed bed	equation (8)
d_t(m)	7.1×10^{-3}	equivalent diameter of the reactor	equation (9)
m(kg)	5×10^{-4}	weight of catalysts	
V_{b1}(m^3)	1.2×10^{-6}	bulk volume of FER catalyst	
V_{b2}(m^3)	6×10^{-7}	bulk volume of CuZnAl catalyst	
V_{p1}(m^3·kg^{-3})	3×10^{-4}	specific pore volume of FER catalyst	
V_{p2}(m^3·kg^{-3})	2×10^{-4}	specific pore volume of CuZnAl catalyst	
ε_{BM1}	0.63	void fraction correction of first stage of the fixed bed	equation (10)
ε_{BM2}	0.67	void fraction correction of second stage of the fixed bed	equation (10)
R_{eM1}	0.59	Reynolds Number in the FER catalyst layer	equation (1)
R_{eM2}	0.82	Reynolds Number in the CuZnAl catalyst layer	equation (1)
L_1(m)	3.0×10^{-2}	height of the FER catalyst bed	
L_2(m)	1.5×10^{-2}	height of the CuZnAl catalyst bed	
Δp_1(Pa)	0.19	pressure drop of the FER catalyst layer	equation (11)
Δp_2(Pa)	0.12	pressure drop of the CuZnAl catalyst layer	equation (11)
Δp(Pa)	0.31	pressure drop of the total catalyst bed	

First stage of the reactor: Feed gas: Ar/DME/CO = 3/4/93 (20 mL/min), T = 493 K, 1.5 MPa, Zeolite weight = 0.5 g; Second stage of the reactor: Feed gas: Ar/DME/CO = 3/4/93 (20 mL/min), 100% H_2 (20 mL/min), T = 493 K, 1.5 MPa, CuZnAl catalyst = 0.5 g.

Journal Name

ARTICLE

Notes and references

1   J. Gong, H. Yue, Y. Zhao, S. Zhao, L. Zhao, J. Lv, S. Wang and X. Ma, *J. Am. Chem. Soc.*, 2012, **134**, 13922–13925.
2   H. T. Luk, C. Mondelli, D. C. Ferré, J. A. Stewart and J. Pérez-Ramírez, *Chem. Soc. Rev.*, 2017, **46**, 1358–1426.
3   Y. Zhu, X. Kong, X. Li, G. Ding, Y. Zhu and Y.-W. Li, *ACS Catal.*, 2014, **4**, 3612–3620.
4   Y. Sun and J. Cheng, *Bioresour. Technol.*, 2002, **83**, 1–11.
5   D. Pimentel and T. W. Patzek, *Nat. Resources Res.*, 2005, **14**, 65–76.
6   P. Ai, M. Tan, N. Yamane, G. Liu, R. Fan, G. Yang, Y. Yoneyama, R. Yang and N. Tsubaki, *Chem.-Eur. J.*, 2017, **23**, 8252–8261.
7   P. Ai, M. Tan, Y. Ishikuro, Y. Hosoi, G. Yang, Y. Yoneyama and N. Tsubaki, *ChemCatChem*, 2017, **9**, 1067–1075.
8   Y. Choi and P. Liu, *J. Am. Chem. Soc.*, 2009, **131**, 13054–13061.
9   R. Zhang, M. Peng and B. Wang, *Catal. Sci. Technol.*, 2017, **7**, 1073–1085.
10 M. J. Chen, H. M. Feder and J. W. Rathke, *J. Am. Chem. Soc.*, 1982, **104**, 7346–7347.
11 P. Cheung, A. Bhan, G. J. Sunley and E. Iglesia, *Angew. Chem. Int. Ed.*, 2006, **45**, 1617–1620.
12 A. Bhan, A. D. Allian, G. J. Sunley, D. J. Law and E. Iglesia, *J. Am. Chem. Soc.*, 2007, **129**, 4919–4924.
13 P. Cheung, A. Bhan, G. J. Sunley, D. J. Law and E. Iglesia, *J. Catal.*, 2007, **245**, 110–123.
14 T. He, X. Liu, S. Xu, X. Han, X. Pan, G. Hou and X. Bao, *J. Phys. Chem. C*, 2016, **120**, 22526–22531.
15 J. Liu, H. Xue, X. Huang, P.-H. Wu, S.-J. H, S.-B. Liu and W. Shen, *Chin. J. Catal.*, 2010, **31**, 729–738.
16 D. B. Rasmussen, J. M. Christensen, B. Temel, F. Studt, P. G. Moses, J. Rossmeisl, A. Riisager and A. D. Jensen, *Angew. Chem. Int. Ed.*, 2015, **54**, 7261–7264.
17 X. Li, X. Liu, S. Liu, S. Xie, X. Zhu, F. Chen and L. Xu, *RSC Adv.*, 2013, **3**, 16549–16557.
18 S. Y. Park, C.-H. Shin and J. W. Bae, *Catal. Commun.*, 2016, **75**, 28–31.
19 Y. Liu, N. Zhao, H. Xian, Q. Cheng, Y. Tan, N. Tsubaki and X. Li, *ACS Appl. Mater. Interfaces,* 2015, **7**, 8398–8403.
20 S. Wang, W. Guo, L. Zhu, H. Wang, K. Qiu and K. Cen, *J. Phys. Chem. C*, 2015, **119**, 524–533.
21 C. Cheng, H. Zhang, W. Ying and D. Fang, *Korean J. Chem. Eng.*, 2011, **28**, 1511–1517.
22 S. Wang, S. Yin, W. Guo, Y. Liu, L. Zhu and X. Wang, *New J. Chem.*, 2016, **40**, 6460–6466.
23 J. Liu, H. Xue, X. Huang, Y. Li and W. Shen, *Catal. Lett.*, 2010, **139**, 33–37.
24 X. Li, X. San, Y. Zhang, T. Ichii, M. Meng, Y. Tan and N. Tsubaki, *ChemSusChem*, 2010, **3**, 1192–1199.
25 Y. Zhang, X. San, N. Tsubaki, Y. Tan and J. Chen, *Ind. Eng. Chem. Res.*, 2010, **49**, 5485–5488.
26 G. Yang, X. San, N. Jiang, Y. Tanaka, X. Li, Q. Jin, K. Tao, F. Meng and N. Tsubaki, *Catal. Today*, 2011, **164**, 425–428.
27 D. Wang, G. Yang, Q. Ma, Y. Yoneyama, Y. Tan, Y. Han and N. Tsubaki, *Fuel*, 2013, **109**, 54–60.
28 P. Lu, G. Yang, Y. Tanaka and N. Tsubaki, C*atal. Today*, 2014, **232**, 22–26.
29 Q. Wei, G. Yang, X. Gao, L. Tan, P. Ai, P. Zhang, P. Lu, Y. Yoneyama and N. Tsubaki, *Chem. Eng. J.*, 2017, **316**, 832–841.
30 F. Yaripour, F. Baghaei, I. Schmidt and J. Perregaard, *Catal. Commun.*, 2005, **6**, 147–152.
31 S. Kumar, S. N. Upadhyay and V. K. Mathur, *Ind. Eng. Chem. Process Des. Dev.*, 1977, **16**, 1–8.
32 P. N. Dwivedi, S. N. Upadhyay, *Ind. Eng. Chem. Process Des. Dev.*, 1977, **16**, 157–165.
33 M. J. Rhodes, *John Wiley & Sons,* England, 2008.
34 N. L. Carr, R. Kobayashi and D. B. Burrows, *J. Pet. Technol*, 1954, **6**, 47–55.
35 Y. Xiao, L. Gao, G. Xiao, B. Fu and L. Niu. *Ind. Eng. Chem. Res.*, 2012, **51**, 11860–11865.
36 CO. Crane, *Technical paper No. 410M,* New York, 1982.

Catalysis Science & Technology Accepted Manuscript

A novel dual bed reactor packed with H-Ferrierite and CuZnAl catalyst for the efficient ethanol synthesis from DME and syngas.

(a) Conventional dual bed reactor   (b) Novel dual bed reactor